Journal of the Australian Ceramic Society (2021) 57:971–981
https://doi.org/10.1007/s41779-021-00600-6

RESEARCH

Physical, structural, and gamma ray shielding studies on novel (35+x) PbO-5TeO_2-20Bi_2O_3-(20-x) MgO-20B_2O_3 glasses

Haifa A.Al-Yousef[1] · Mohammed Alotiby[2] · Ashok Kumar[3,4] · B. M. Alotaibi[1] · N. A. M. Alsaif[1] · M. I. Sayyed[5,6] · K. A. Mahmoud[7,8] · Y. Al-Hadeethi[9]

Received: 19 December 2020 / Revised: 18 March 2021 / Accepted: 2 April 2021 / Published online: 13 April 2021

Abstract

The primary aim of this investigation is to synthesize a novel glass system with a composition (35+x) PbO-5TeO_2-20Bi_2O_3-(20-x) MgO-20B_2O_3 (where x=0, 5, 10, 15, and 20 mol%) by melt quenching method. The confirmation of the amorphous behavior and the presence of the various vibration modes and stretching modes have been analyzed using the XRD and FTIR techniques, respectively. The radiation shielding parameters of these glasses were reported using MCNP5 simulation. The effects of PbO on the MCNP5 parameters were investigated in detail. The mass attenuation coefficient (MAC) was simulated via MCNP5 code, and it was found that the MAC values from MCNP5 all follow the same trend as the XCOM data. The similarity means that the two simulations strongly agree with each other. The linear attenuation coefficient (LAC) was calculated for all the glasses. The glass sample with 55 mol% of the PbO has the greatest LAC at any energy, such as 0.317 at 10 MeV, the lowest investigated energy. From the LAC values, other parameters such as transmission factor (TF), lead equivalent thickness (d_{lead}), and half-value layer (HVL) were reported. The results for the TF of the glasses revealed that the glass systems become more effective as their thickness increases. Glass sample with 35 mol % of the PbO recorded the highest TF at all energies due to its lack of PbO content, such as 15.533% for a thickness of 1 cm and 6.122% for 1.5-cm thickness at 0.3 MeV. The radiation protection efficiency (RPE) was also determined, and we found that the glasses with the greater PbO content and least MgO content have the highest RPE. Therefore, based on the RPE values, glasses with the greater PbO are the most effective radiation shield from the investigated glasses.

Keywords Heavy metal oxide borate glass · Shielding · MCNP5 · FTIR

Introduction

Technologies that use radiation to function properly are becoming increasingly prominent. Ionizing radiation has enough energy to detach electrons from atoms, whereas non-ionizing radiation does not. Ionizing radiation is used in the dental and other fields, for example, in X-ray imaging machines for radiography. It is also used in other fields such as agriculture and energy generation. Although ionizing radiation is widely used

✉ Mohammed Alotiby
mfotiby@kacst.edu.sa

✉ M. I. Sayyed
mabualssayed@ut.edu.sa

[1] Department of Physics, College of Science, Princess Nourah bint Abdulrahman University, Riyadh, Saudi Arabia

[2] King Abdulaziz City for Science and Technology, Riyadh, Saudi Arabia

[3] University College, Benra, Dhuri, Punjab 148024, India

[4] Department of Physics, Punjabi University, Patiala, Punjab 147002, India

[5] Department of Physics, Faculty of Science, Isra University, Amman 11622, Jordan

[6] Department of Nuclear Medicine Research, Institute for Research and Medical Consultations, Imam Abdulrahman Bin Faisal University, Dammam 31441, Saudi Arabia

[7] Ural Federal University, Mira St., 19, 62002 Yekaterinburg, Russia

[8] Nuclear Materials Authority, El Maadi, Cairo, Egypt

[9] Department of Physics, Faculty of Science, King Abdulaziz University, Jeddah 21589, Saudi Arabia

for its many benefits, human exposure to this type of radiation can have serious consequences [1–5].

Long-term exposure to the radiation may cause nausea, vomiting, cancer, and even death. In order to prevent excessive exposure of workers and patients who must contact radiation, it is advised to both limit the time under exposure and remain as far away from the source as possible. However, in some cases, these two guidelines would not be sufficient to keep people from experiencing these side effects. Thus, radiation shielding materials are used to provide more protection levels and absorb incoming photons [6–9].

Radiation shields reduce the amount of radiation the person is exposed to. The radiation shield aims to attenuate or absorb as much radiation as possible to reduce the intensity of the incoming photons to safe levels [10]. Various kinds of materials are often used as radiation shields depending on the application. Concrete is utilized in this regard because of its sturdiness and low cost [11]. Although concrete is a versatile and effective material, it is prone to cracking and losing its water content when exposed to high radiation levels. Other materials such as alloys are often used. Alloys are a mixture of multiple metals that can often be highly effective. Another material has gained recent attention due to its unique properties [12].

Glasses are used as radiation shields because of their easily modifiable characteristics, low cost, and transparency, a property unique to glass [13–16]. They can be used in X-ray rooms, for instance, to allow workers to view inside the room where the patient is. Glasses can be doped with metal oxides or HMOs, heavy metal oxides to improve their attenuation properties. Common glass formers include borate and silicate. Borate offers good chemical resistance when used as a glass former due to its BO_3 units. The addition of glass modifiers, which are oxides that alter the properties of the glass, can convert some of the BO_3 units into tetrahedral BO_4 units. This transformation creates non-bridging oxygens (NBOs), which can alter the glass's physical properties. Alkali and alkaline earth elements are common examples of glass modifiers [17].

Other oxides act as intermediates, which can function as glass formers or modifiers depending on the glass system's composition. Some examples of intermediates include tellurium, lead, and bismuth. When combined with borate, bismuth improves the optical transparency, rate of crystallization, and refractive index of the glass. These properties make Bi_2O_3 useful in thermal and mechanical sensors and scintillation detectors. Additionally, all three of these intermediates also have a high density, which previous research has shown to have a positive correlation with attenuation. Lead is especially useful because of its accessibility and effectiveness as a radiation shield [18, 19].

To understand the ability of a medium to attenuate radiation, some factors are calculated and evaluated. Typically, experimental methods are used to obtain these parameters; however, due to the lack of facilities currently available because of the COVID-19 pandemic, alternative methods are necessary to determine these parameters. Theoretical approaches using some computer programs are often used to check the accuracy of radiation shielding experiments and have proven to be highly accurate in previous studies as an alternative method. Phys-X computer software specifically has been found to be acceptable because of its ability to calculate different shielding variables accurately. In our recent paper, we have reported the preparation and investigations of the optical and the mechanical properties of the PbO-TeO_2-Bi_2O_3-MgO-B_2O_3 glass system. Also, we reported the gamma ray shielding behavior of the aforementioned glasses using the FLUKA code from 0.1218 to 1.405 MeV [20]. In continuation of the work, the present studies used MCNP5 code to investigate the radiation shielding ability of PbO-$5TeO_2$-$20Bi_2O_3$-(20-x) MgO-$20B_2O_3$ glasses. In addition to this, the detailed study of physical and structural properties has also been discussed.

Materials and methods

Glass preparation and characterization

The glass samples were fabricated with nominal composition of (35+x) PbO-$5TeO_2$-$20Bi_2O_3$-(20-x) MgO-$20B_2O_3$ (where x=0, 5, 10, 15, and 20 mol% and are denoted PTBMB35, PTBMB40, PTBMB45, PTBMB50, and PTBMB55, respectively). The specific weights of the powders of analytical reagent-grade chemicals were utilized in the current investigation. The melt quenching technique prepares the glass samples. Firstly, the appropriate amounts of homogeneously mixed samples were taken in an alumina crucible and melted in an electronic furnace at 1030 °C for 1 h. The melted mixture was then poured in a graphite mold and annealed at 300 °C for 2 h to remove residual thermal strain and then allowed to cool the room temperature for a period of 24 h. A picture of the fabricated glasses is given in Fig. 1. The density of the samples was determined via the Archimedes' Principle [20, 21]. The composition of the tested samples has been listed in Table 1. The appropriate amounts of these powdered samples are taken for different characterization studies of XRD and FTIR spectroscopy, respectively. The details of the instrumentation and the formulations used for the physical and the structural studies have been discussed in detail in our previous studies [21–25].

Gamma ray shielding capacity determination

MCNP5 code is a valuable and helpful code to estimate the projected photons' average track length in the fabricated samples. For good and accurate simulation data, geometry should

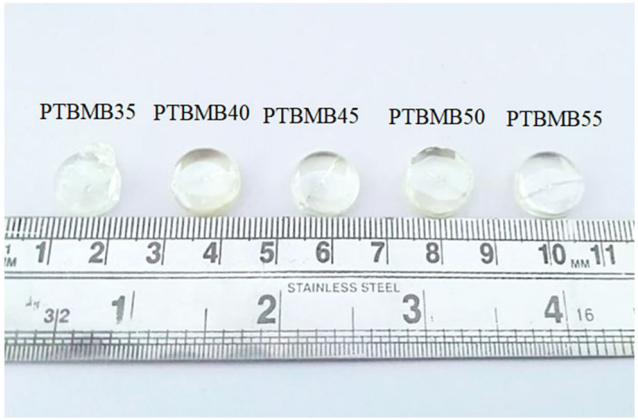

Fig. 1 A picture for the fabricated glasses

be performed. In the present study, the geometry was arranged to be similar to the experimental measurement, as exhibited in Fig. 2. The photon source was placed in the center of the organized geometry and surrounded by a lead collimator to collimate the projected photon flux. After that, the collimated photon flux was directed to the fabricated glass samples. After the gamma flux interaction with the fabricated material, the photon flux transmitted the glass thickness and headed to the detector. It was arranged to be an F4 tally to estimate the detector's average flux per unit cell. The MCNP-5 code was connected with the primary cross-section data sources ENDF, ACTI, ...etc files [26]. The NPS card is arranged to be 10^6 historical/min. It is important to state that the output file recorded a relative error of less than 1%.

XCOM is an online software program; it has the ability to calculate different shielding variables accurately in the energy range between 1keV to 1 GeV. The requirement of the mentioned program to calculate the MAC is the composition of the tested sample in wt% and the gamma photon energies [27].

Results and discussion

This work has been classified into various subsections. The subsections describe the physical, structural, and radiation shielding features for the tested PTBMB samples as follows:

Table 1 Chemical composition of the present samples

Glass code	Glass composition (mol %)					Density (g/cm^3)
	TeO_2	Bi_2O_3	PbO	MgO	B_2O_3	
PTBMB35	5	20	35	20	20	5.09
PTBMB40	5	20	40	15	20	5.36
PTBMB45	5	20	45	10	20	5.49
PTBMB50	5	20	50	5	20	6.1
PTBMB55	5	20	55	0	20	6.21

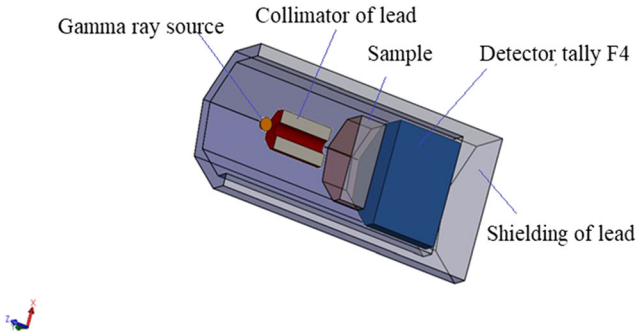

Fig. 2 The MCNP5 set up

Physical properties

Table 2 describes the several physical properties of the selected glass system. The density value of the selected PTBMB glasses changes from 5.09 to 6.21 g/cm^3 with an increase in contents of PbO in the glass systems because of the higher atomic mass of lead which accounts for the increment in the average molecular weight of the selected glass systems. The increase in density implies the compactness of the samples with an increase in contact of PbO. The molecular mass of the samples is increasing from 201.27 to 237.85 g/mol. The molar volume (V_m) decreases from 39.58 to 38.30 cm^3 as the amount of PbO increases resulting in the sample's compactness. This trend may be due to the creation of non-bridging oxygen atoms [28]. The ion concentration (N) increases from $5.33 \times 10^{+21}$ to $5.5 \times 10^{+21}$ ions/cm^3 with an increase in the amount of PbO. The volume of boron atoms per mole (V_m^b) decreases from 24.71 to 23.93 cm^3. The average boron-boron separations ($<d_{b-b}>$) are decreasing from 3.45×10^{-8} to 3.41×10^{-8} m with increasing in the concentration of PbO. The decrease in separation indicates that the glass structures are compact, and the density of the glass systems is increasing. The polaron radius (r_p) value reduces from 2.31×10^{-8} to 2.28×10^{-8} m [29]. A similar indication is given by the internuclear distance (r_i) as it also decreases from 5.72×10^{-8} to 5.66×10^{-8} m [29]. The field strength (F) rises from 5.64×10^{15} to 5.76×10^{15} cm^{-2} with a rise in the mol% of PbO from 35 to 55%.

Structural properties

In Fig. 3 we exhibits the XRD profiles of selected glasses. The non-occurrence of sharp peak indicates the non-existence of the crystalline structure. The presence of broadband is due to the diffused X-ray scattering.

FTIR spectra in the absorbance mode have been represented in Fig. 4. Evidently, the borate groups play a dominant role in the IR spectra. A band around ~411cm^{-1} represents the vibrations of metal cations in their oxygen sites and respective tetrahedral [30]. The other three bands around ~480 cm^{-1} represent the stretching vibration in

Table 2 Physical properties of the present samples

Physical properties	PTBMB35	PTBMB40	PTBMB45	PTBMB50	PTBMB55
Ddensity (g/cm^3)	5.09	5.36	5.49	6.1	6.21
M (g)	201.27	210.42	219.56	228.71	237.85
V_m (cm^3)	39.54	39.26	39.99	37.49	38.30
N (ions/cm^3)	5.33 E+21	5.37 E+21	5.27 E+21	5.62 E+21	5.5 E+21
V_m^b (cm^3)	24.71	24.54	24.99	23.43	23.93
$<d_{b\text{-}b}>$ (m)	3.45 E−08	3.44 E−08	3.46 E−08	3.39 E−08	3.41 E−08
r_p (m)	2.31 E−08	2.3 E−08	2.32 E−08	2.27 E−08	2.28 E−08
r_i (m)	5.72 E−08	5.71 E−08	5.75 E−08	5.62 E−08	5.66 E−08
F(cm^{-2})	5.64 E+15	5.67 E+15	5.6 E+15	5.84 E+15	5.76 E+15

PbO_4 groups [31]. There are small bands around ~639 cm^{-1}, ~646 cm^{-1}, and ~670 cm^{-1} that may be due to Pb–O bond vibrations of PbO_n units with n = 3 and/or 4 [31]. There are small bands around ~892 cm^{-1} that may be due to the symmetric stretching of BO_4 units [32]. The two IR bands approximately ~935 cm^{-1} and ~936 cm^{-1} represent the B-O stretching vibrations of tetragonal (BO_4) units in diborate groups [32]. Small other bands like ~1223 cm^{-1} and ~1229 cm^{-1} may be due to B-O stretching vibrations of [BO_3] unit orthoborate groups [30]. The small bands are observed ~1310 cm^{-1}, and ~1317 cm^{-1} represents B−O bond stretching vibration of BO_3 units in metaborate, pyroborate, and orthoborate groups [33]. The other IR bands ~1363 cm^{-1} and ~1364 cm^{-1} may be due to asymmetric stretching modes of BO_3 and BO_2O^- unit [32]. The IR spectra of selected glasses possess three broad transmittance IR bands at 600–800 cm^{-1} due to bending vibrations of B-O atoms between trigonal boron atoms, 800–1200 cm^{-1} due to the stretching of B–O bond of the tetrahedral BO_4 units, and 1200–1500 cm^{-1}due to the asymmetric stretching relaxation of B-O bond of trigonal BO_3 units with NBOs [22, 34].

Radiation shielding investigation

The MAC of the five glasses is listed in Table 3. Two simulation programs were used to obtain the MACs, MCNP5, and XCOM. The MACs were calculated between 0.015 and 15 MeV. The values from the MCNP5 code all follow the same

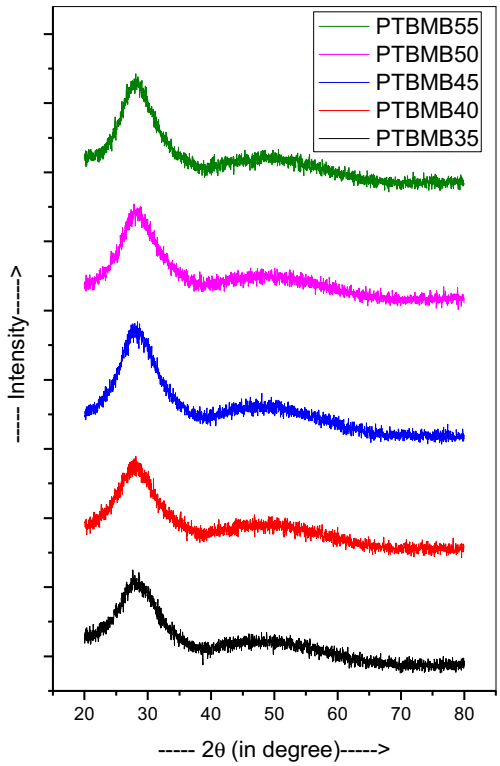

Table 3 The mass attenuation coefficient (cm^2/g) for the prepared samples obtained by MCNP5 and XCOM

Energy (MeV)	PTBMB35			PTBMB40			PTBMB45			PTBMB50			PTBMB55		
	MCNP5	XCOM	diff (%)	MCNP5	XCOM	diff (%)	MCNP5	XCOM	diff (%)	MCNP5	XCOM	diff (%)	MCNP5	XCOM	diff (%)
0.015	90.253	90.400	0.162	91.774	91.930	0.170	93.166	93.330	0.176	94.443	94.620	0.187	95.630	95.810	0.189
0.03	24.322	24.340	0.075	24.751	24.770	0.079	25.143	25.170	0.106	25.505	25.530	0.097	25.839	25.860	0.082
0.05	6.752	6.783	0.455	6.851	6.882	0.456	6.941	6.973	0.463	7.024	7.057	0.469	7.101	7.134	0.468
0.08	2.018	2.055	1.858	2.045	2.083	1.839	2.071	2.110	1.886	2.094	2.134	1.887	2.116	2.156	1.882
0.3	0.366	0.344	5.973	0.370	0.348	5.911	0.377	0.352	6.570	0.378	0.356	5.812	0.381	0.359	5.798
0.5	0.147	0.147	0.026	0.151	0.148	2.572	0.153	0.149	3.098	0.154	0.150	3.087	0.155	0.150	3.042
0.8	0.085	0.085	0.560	0.085	0.085	0.572	0.085	0.086	0.575	0.085	0.086	0.579	0.086	0.086	0.587
1	0.067	0.070	3.671	0.067	0.070	3.724	0.067	0.070	3.790	0.067	0.070	3.833	0.067	0.070	3.879
3	0.041	0.041	0.891	0.041	0.041	0.896	0.041	0.041	0.920	0.041	0.041	0.909	0.041	0.041	0.936
5	0.040	0.040	0.408	0.040	0.040	0.411	0.040	0.040	0.407	0.040	0.040	0.415	0.040	0.040	0.409
8	0.042	0.042	0.213	0.042	0.042	0.222	0.043	0.043	0.227	0.043	0.043	0.219	0.043	0.043	0.217
10	0.044	0.044	0.171	0.044	0.044	0.167	0.045	0.045	0.174	0.045	0.045	0.154	0.045	0.045	0.169
15	0.049	0.049	0.110	0.050	0.050	0.117	0.050	0.050	0.110	0.050	0.051	0.120	0.051	0.051	0.119

trend as the XCOM software. The similarity means that the two approaches used for the determination of the MAC agree with each other. For PTBMB35 (as an example) and at 0.05 MeV, the MAC values obtained by MCNP5 and XCOM are, respectively, 6.752 and 6.783 cm^2/g (the difference as given in Table 3 is 0.026%). For higher energy and for another sample (0.8 MeV and for PTBMB50 glass), the MCNP5 and XCOM are 0.067 and 0.070 cm2/g (with a difference of around 3%). For any prepared glass and at all selected energies, the MCNP5 and XCOM values show a good agreement. Also, from Table 3, the five glasses' MAC values can be noticed to reduce as energy increases. The MACs can be observed to decline sharply for low energies, slowing down and decreasing at a steady pace as energy increases. At 0.015 MeV, the MAC of PTBMB35 is equal to 90.253 cm^2/g, at 0.08 MeV, it is equal to 2.018 cm^2/g, while for E=5 MeV, its MAC is 0.04 cm^2/g.

The LAC for the five glasses was graphed against photon energy plus the PbO content in Fig. 5. The same photon energy range used in the MAC was chosen in Fig. 5. Two main trends can be noticed when examining the figure, trends that can also be applied to the MACs in Table 3. First, at all photon energies, LAC decreases as energy increases for all five glasses. This trend can be subdivided into three sections. The first energy region, region a, between 0.015 and 0.3 MeV, is the range where the photoelectric effect is influential. A sharp decrease in the LAC values can be observed in the region a. For instance, at this low-energy region, the LAC of the PTBMB35 glass decreases from 459.390 to 1.862 cm^{-1} between 0.015 and 0.3 MeV. At higher energies, namely, between 0.5 and 3 MeV, the LAC relatively remains constant, decreasing slowly as energy increases. For example, at 0.5 MeV, PTBMB35 has a LAC of 0.746 cm^{-1}, and PTBMB40 has a LAC of 0.812 cm^{-1}, whilstfor PTBMB45, the LAC is 0.842 cm^{-1}. This region (say region b) is dominated by Compton scattering, another photon interaction phenomenon, which is responsible for the slighter decrease in values. For E>3 MeV, a new photon interaction phenomenon becomes important, namely, pair production, and we found a very slight increase in the LAC between 5 to 15 MeV. The other trend comes from the content of PbO of the glasses. At any energy, PTBMB55, which has the greatest amount of PbO, has the greatest LAC, while PTBMB35, with the least amount of PbO (35 mol%), has the lowest LAC. At 0.03 MeV (as an

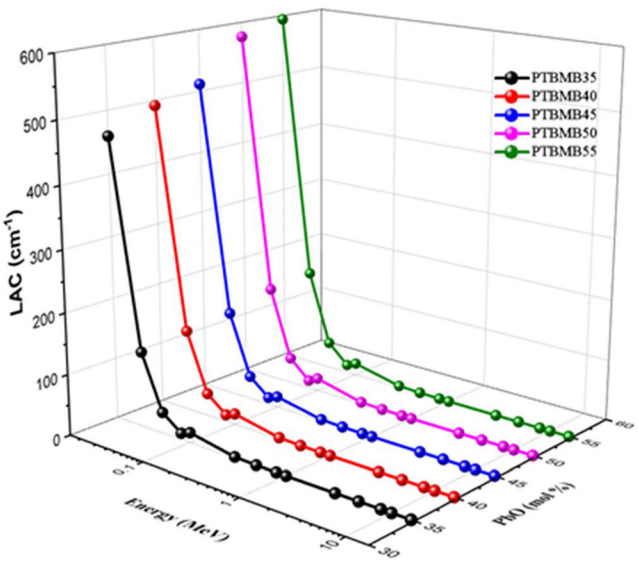

Fig. 5 The LAC of the fabricated glasses versus energy

example), PTBMB35 has a LAC of 123.798 cm^{-1}, and PTBMB55 has a LAC of 160.460 cm^{-1}. Even though this difference is maintained at all energies, the difference between the values largely decreases at higher energies (see Fig. 6). The observed difference between the LAC values in Fig. 6 is related to the glass-effective atomic number variation with increasing the PbO incrementations. The photon interaction cross-section varied with Z^{4-5}, Z, and Z^2 for photon electric, Compton scattering, and pair production interactions, respectively. Thus, at the low-energy zone (e.g., 0.015 MeV), the photoelectric is prevailing. The LAC variation at 0.015 MeV is higher than the other two energies (0.3 for Compton scattering and 15 MeV for pair production interaction) when the PbO increased between 35 and 55 mol%. For instance, when the photon energy is 15 MeV, PTBMB35 has a LAC of 0.250 cm^{-1}, PTBMB40 has a LAC of 0.266 cm^{-1}, PTBMB45 has a LAC of 0.275 cm^{-1}, while for PTBMB50 and PTBMB55, LAC values are, respectively, 0.308 and 0.316 cm^{-1}. As can be seen, the values are much closer together. From this parameter, PTBMB55 offers the superior radiation attenuation potential among the PTBMB samples. At higher energies, the shielding abilities of the glasses are quite similar. Thus, it can be concluded that the amount of PbO in this glass system has a significant role on the shielding competence at lower energy while only having a slight impact at higher energies.

Figure 7 presents a comparison between the tested glasses LAC and those of some commercial and previously manufactured lead-based glasses like RS 360, RS 520, and LBPCu0 at 0.662 MeV [35, 36]. The LAC of the tested glass samples is ranged between 0.5236 and 0.6493 cm^{-1} at gamma photon energy 0.662 MeV. The mentioned values of LAC are higher than that reported for glasses RS 360, RS520, and LBPCu0. The LAC for glasses RS 360, RS520, and LBPCu0 at 0.662 MeV is 0.32, 0.52, and 0.345, respectively.

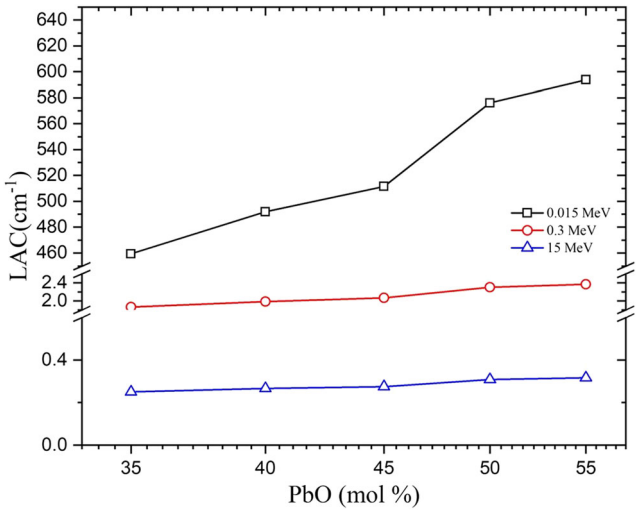

Fig. 6 The LAC of the present samples versus PbO content

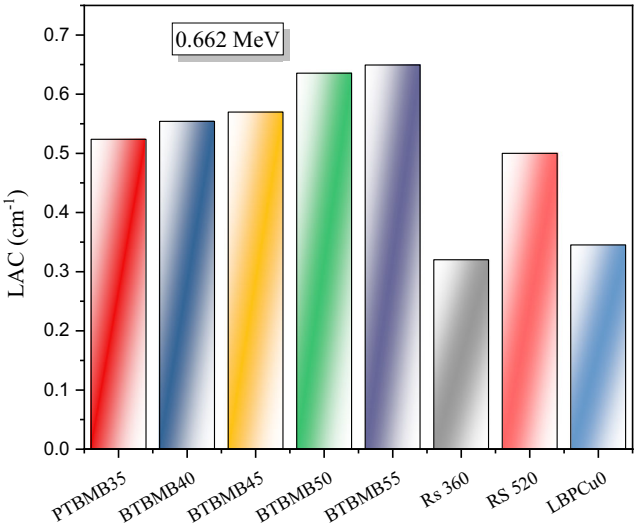

Fig. 7 Comparison between the LAC of the present samples with different standard shielding glasses (RS 320 and RS 520) and previously lead-based glass

The half-value layer (HVL) for the PTBMB glasses with different concentrations of PbO was investigated and plotted in Fig. 8a. The HVL starts with a small value until E=0.1 MeV, where it starts to increase quickly. It is found from Fig. 8a that the HVL for PTBMB35 changes from 0.002 (at 0.015 MeV) to 0.043 cm (at 0.1 MeV), and to 3.252 cm (at 8 MeV). The same increase behaviour in the HVL is reported for the other glasses. From these values, one can conclude that a greater thickness of the medium is required to decline the energy of the incident photons by 50%. The figure reveals that HVL decreases as the PbO changes from 0 to 20 mol%. This relationship is due to the inverse relationship between density and HVL; as the amount of PbO increases, the density of the glass diminishes, decreasing HVL. Since a lower HVL signifies a more effective shield, the figure indicates that the greater the PbO content, the better the glass will be as a radiation shield. In Fig. 8b, c, and d, we calculated the average HVL in low-, moderate-, and high-energy zones and plotted the results as a function of the content of PbO. In the three mentioned zones, the average HVL decreases with increasing the PbO content. The HVL is varied between 0.0217 and 0.0275 cm at the low-energy zone, varied between 1.578 and 1.955 cm for the moderate-energy zone, and varied between 2.415 and 3.043 cm for the high-energy zone.

Transmission factor (TF) for the PTBMB glasses is investigated. It is noteworthy to remember that a lower TF means a more efficient radiation shield. The fabricated glass TF was plotted in Fig. 9 versus the glass thicknesses at different gamma photon energies. The chosen thicknesses varied between 0.5 and 2 cm, representing a variety of thinner and thicker samples. The subfigures demonstrate a reducing behaviour as energy increases. Since more radiation can penetrate

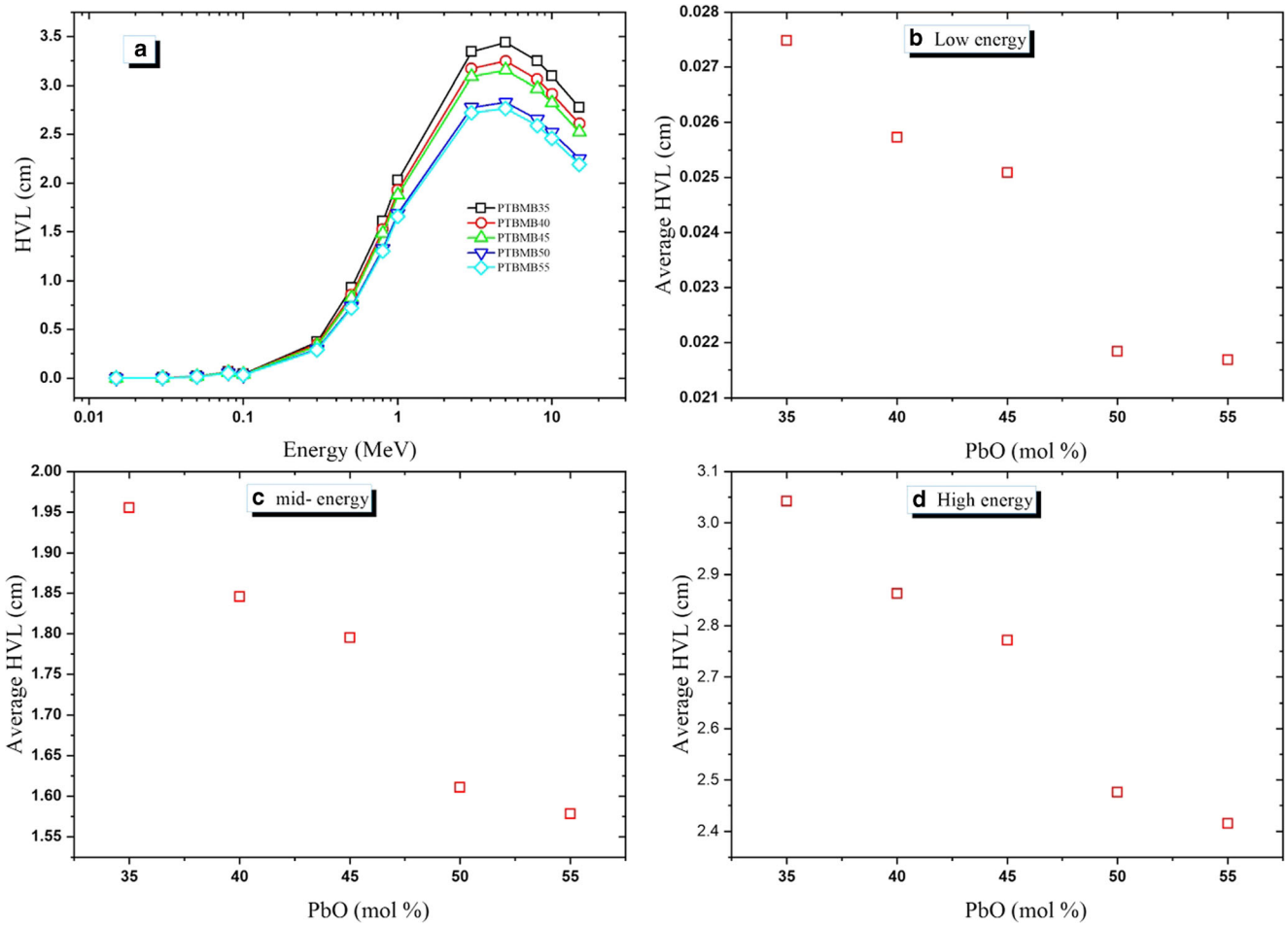

Fig. 8 The HVL versus energy and PbO content

through the sample at higher energies, the ratio increases, increasing TF. For PTBMB55, the minimum values for TF, which occur at 0.3 MeV, are 30.617, 9.374, 2.870, and 0.879% for 0.5, 1, 1.5, and 2 cm, respectively. This glass's maximum values occur at the greatest energy, 15 MeV, and equal to 85.381, 72.900, 62.243, and 53.144% for the selected thicknesses. Like the LAC values, a greater difference between the TFs can be observed at lower energies, while the values are closer together as energy increases. The figure also demonstrates that the highest the glass's thickness, the lower the TF and the better the shield. Typically, a thicker radiation shield is always more desirable as more collisions can occur between the material and the incoming photons, absorbing the radiation if space is not a major issue. A larger difference between thicker and thinner samples can especially be observed at low energies.

Also, from Fig. 9, we can compare the influence of the PbO presenting in each glass on the TF. Apparently, TF decreases with PbO, implying that a sample with a higher amount of PbO is more effective at stopping radiation. When comparing two different samples at the same energy (let us choose the sample with the lowest and highest PbO), the TF for PTBMB55 is lower than the TF for PTBMB35 for all thicknesses. For 0.3 MeV (Fig. 9a), the TF for 1 cm PTBMB35 is 15.533% and 6.122% for 1.5 cm, while the TF for 1 cm PTBMB55 is 9.374% and 02.870 % for 1.5 cm. This difference indicates that the greater the PbO content in these glasses, the more effective the glass will be as a radiation shield.

Figure 10 demonstrates the RPE of the glasses at the selected thicknesses used in the previous curves and at some energies. A greater RPE typically correlates with a more effective radiation shield since more photons are absorbed. The results indicate a similar trend when compared to LAC. The values increase rapidly with increasing the thickness of the sample. The exact opposite of what we found in the previous figure, RPE continually decreases as energy increases. For instance, PTBMB35 with a thickness of 0.5 cm decreases from 60.59 at 0.3 MeV, to 31.13% at 0.5 MeV, and to 11.73% at 15 MeV. In addition, at all energies, RPE follows the trend of PTBMB35 < PTBMB40 < PTBMB45 < PTBMB50 < PTBMB55, such as at 0.444 MeV, the RPE values at 0.5 MeV are 67.33, 70.42, 71.72, 75.62, and 76.40% for PTBMB35, PTBMB40, PTBMB45, PTBMB50, and PTBMB55, respectively (this is for a

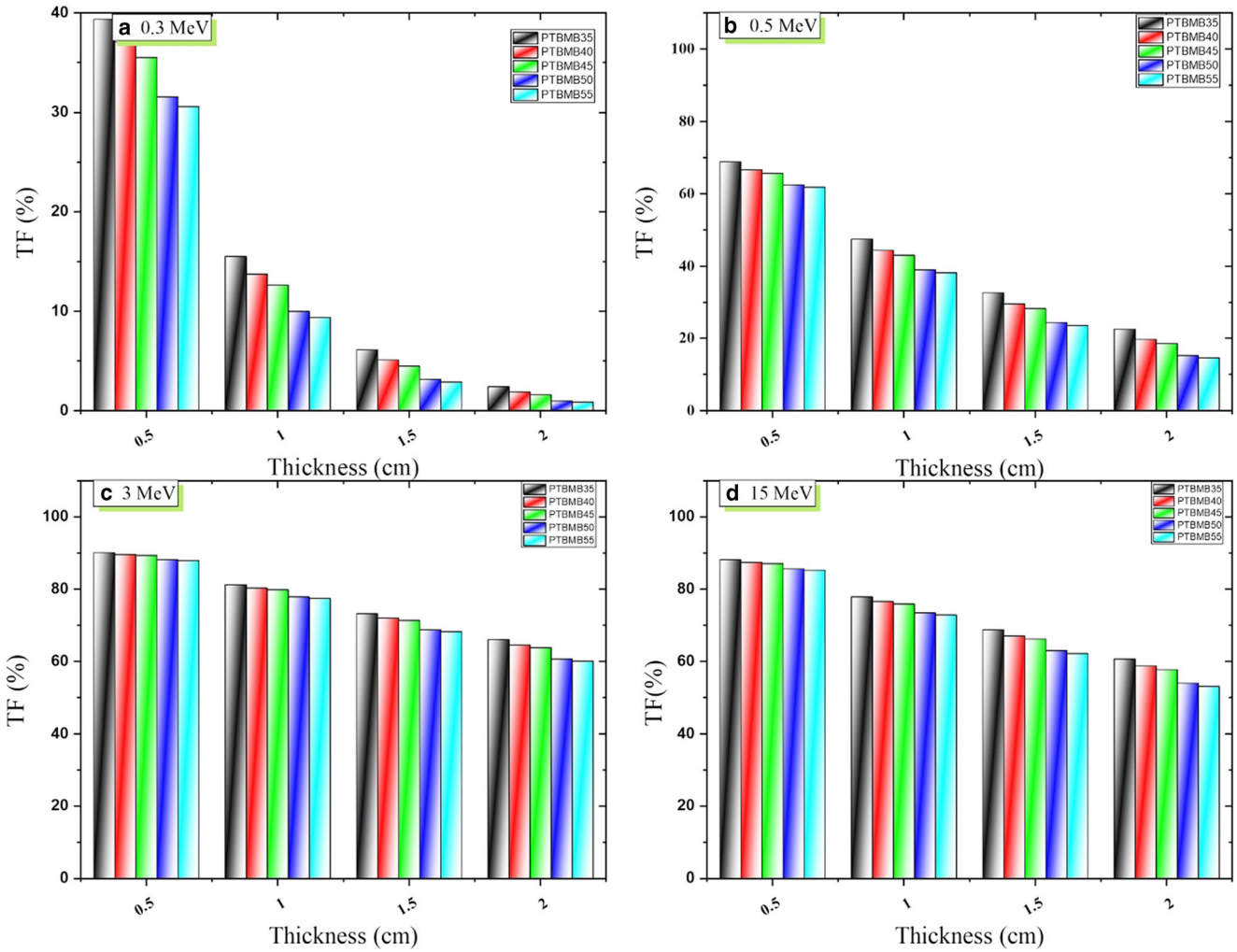

Fig. 9 The TF versus the glass thickness

thickness of 1.5 cm). The samples with the greater PbO content and least MgO content (PTBMB55) have the highest RPE since Pb has a higher atomic number than Mg, so as more PbO replaces the MgO, the RPE increases. Accordingly, the greater the PbO content in the glass system, the better the radiation shield the glass will be. Therefore, based on the RPE values, PTBMB55 is the most efficacious radiation shield out of the tested glasses, which agrees with the other parameters' results.

In addition to TF and RPE, the equivalent lead thickness of the glasses (d_{lead}) was calculated. We calculated each fabricated sample's thickness, which has the same shielding capacity of a Pb with a thickness of 0.5 and 1 cm (see Fig. 11a and b). Apparently, the d_{lead} decreases with the addition of PbO. This result agrees with the data from the TF and RPE. At 0.08 MeV, 1.336 cm of PTBMB35 can attenuate the same radiation level that a 0.5 cm of a lead sample can do. When the PbO content becomes 55 mol% (i.e., PTBMB55), the d_{lead} reduces to 1.044 cm (this is at 0.08 MeV). At this energy, the d_{lead} decreases from 2.671 to 2.087 cm. Generally, the addition of PbO causes a reduction in the d_{lead} which indicates that more PbO is preferable in order to decrease the dimensions of the glass that can shield specific amount of the radiation.

The fast neutron effective removal cross-section (Σ_R) is presented in Fig. 12. The values given in this figure are varied between 0.01637 and 0.01503 $cm^2\ g^{-1}$. As we can see from Fig. 12, the ability of the PTBMB glass to shield the neutrons depends on the content of PbO and MgO. The reduction in the parameter given in Fig. 12 can be explained according to the fact that the low atomic number element (Mg in this work) is better in shielding the neutron than the high atomic number. So, the glass with the maximum MgO content (PTBMB35) owns ;the highest fast neutron effective removal cross-section.

Conclusion

We succeed to synthesize a novel glass system with a composition (35+x) PbO-5TeO_2-20Bi_2O_3-(20-x) MgO-20B_2O_3. The confirmation of amorphous behavior and

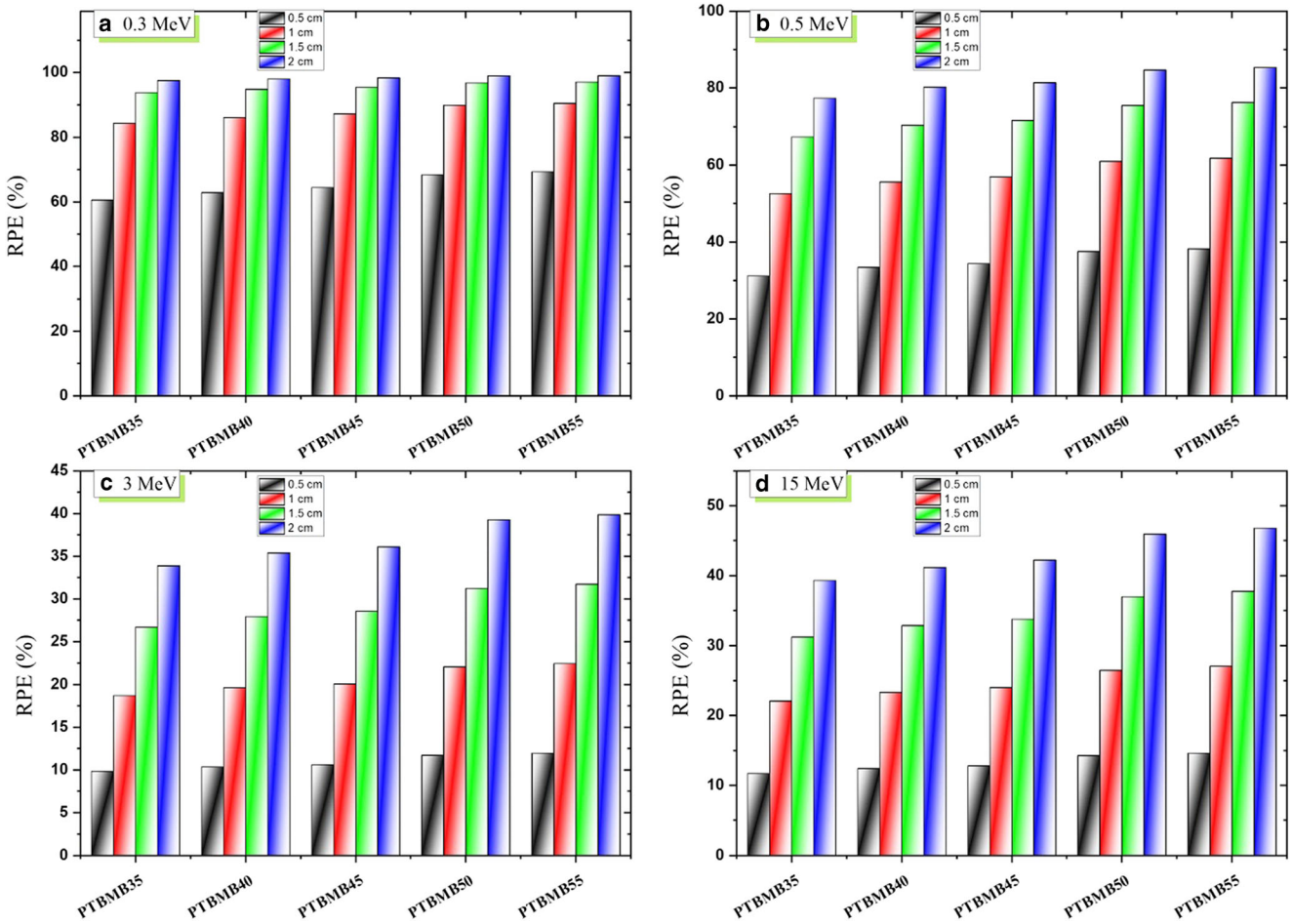

Fig. 10 The radiation protection efficiency for the present samples

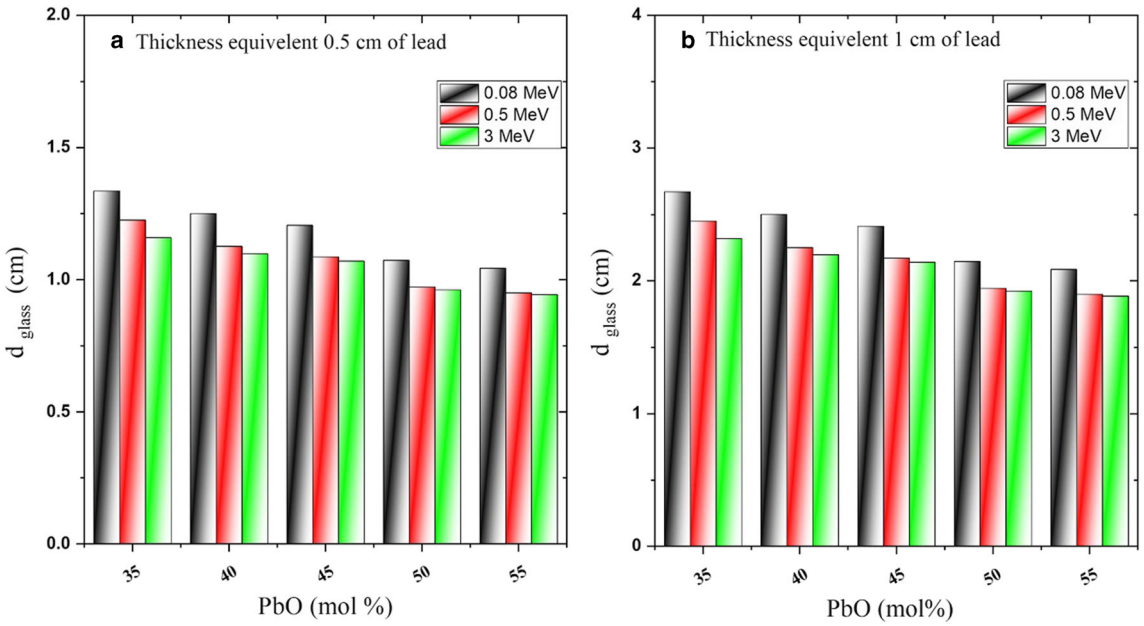

Fig. 11 Variation of the lead-equivalent thickness for the fabricated samples versus the PbO content

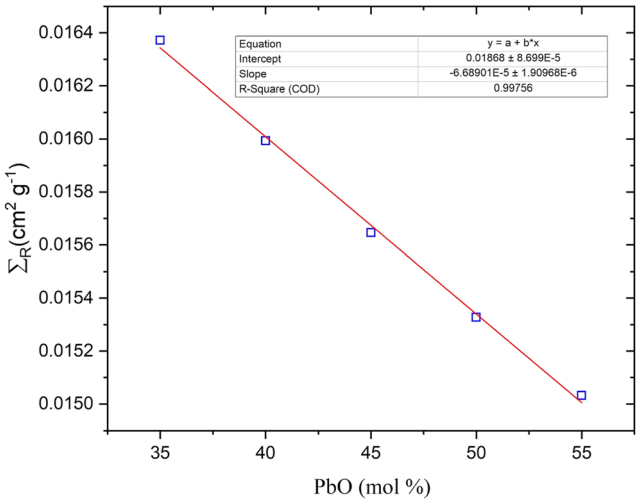

Fig. 12 Variation of the Σ_R versus the PbO content

the presence of the various vibration modes and stretching modes have been analyzed using the XRD and FTIR techniques, respectively. The LAC, TF, RPE, and d_{lead} of the glasses were calculated via the MCNP5 code and suitable formulas. The MAC values were determined using MCNP5 and XCOM simulations, and when compared, it was found that they both greatly agreed with each other. The LACs of the glasses followed the trend of PTBMB35 < PTBMB40< PTBMB45< PTBMB50< PTBMB55. The HVL values tended to decrease as the PbO increased. Also, the HVL values tended to increase as the energy increased, such as PTBMB35 increases from 0.002 (at 0.015 MeV) to 3.252 cm (at 8 MeV). The TF results revealed that the glass systems become more effective as their thickness increases. The results concluded that PTBMB55 was the most effective radiation shield, however, by a smaller margin at higher energies. The addition of PbO in the glasses was determined to have a beneficial effect on the glass system's shielding ability.

Funding This research was funded by the Deanship of Scientific Research at Princess Nourah bint Abdulrahman University through the Fast-Track Research Funding Program.

References

1. Bagheri, R., Hassan, Y.: Alireza Khorrami Moghaddam, Gamma ray shielding study of Barium-Bismuth-Borosilicate glasses as transparent shielding materials using MCNP-4C code, XCOM program, and available experimental data, Nuclear. Eng. Technol. **49**, 216–223 (2017)
2. Mhareb, M.H.A.: Physical, optical and shielding features of Li_2O–B_2O_3–MgO–Er_2O_3 glasses co-doped of Sm2O3. Appl. Phys. A. **126**, 71 (2020)
3. Aljawhara, H., Almuqrin, Sayyed, M.I.: Radiation shielding characterizations and investigation of TeO_2–WO_3–Bi_2O_3 and TeO_2–WO_3–PbO glasses. Appl. Phys. A. **127**, 190 (2021)
4. Al-Hadeethi, Y., Sayyed, M.I.: BaO–Li_2O–B_2O_3 glass systems: potential utilization in gamma radiation protection. Prog. Nucl. Energy. **129**, 103511 (2020)
5. Alajerami, Y.S., Drabold, D., Mhareb, M.H.A.: Katherine Leslee A Cimatu, Gang Chen, Physical, structural and shielding properties of cadmium bismuth borate-based glasses. J. Appl. Phys. **127**, 175102 (2020)
6. Sayyed, M.I., Al-Hadeethi, Y., AlShammari, M.M., Ahmed, Al-Heniti, S.H., Rammah, Y.S.: Physical, optical and gamma radiation shielding competence of newly borotellurite based glasses: TeO_2–B_2O_3–ZnO–Li_2O_3–Bi_2O_3. Ceram. Int. **47**, 611–618 (2021)
7. Dong, M., Xue, X., Kumar, A., He, Y., Sayyed, M.I., Liu, S., Bu, E.: A novel method of utilization of hot dip galvanizing slag using the heat waste from itself for protection from radiation. J. Hazard. Mater. **344**, 602–614 (2018)
8. Singh, V.P., Badiger, N.M.: Shielding efficiency of lead borate and nickel borate glasses for gamma rays and neutrons. Glas. Phys. Chem. **41**, 276–283 (2015)
9. Sayyed, M.I., Mahmoud, K.A., Lacomme, E., AlShammari, M.M., Dwaikat, N., Alajerami, Y.S.M., Alqahtani, M., El-bashir, B.O., Mhareb, M.H.A.: Development of a novel MoO_3-doped borate glass network for gamma-ray shielding applications. Eur. Phys. J. Plus. **136**, 108 (2021). https://doi.org/10.1140/epjp/s13360-020-01011-5
10. Rashid, R.S.M., Mohammed Salem, S., Azreen, N.M., Voo, Y.L., Haniza, M., A.A.: Shukri, Mohd-Syukri Yahya, Effect of elevated temperature to radiation shielding of ultra-high performance concrete with silica sand or magnetite. Constr. Build. Mater. **262**, 120567 (2020)
11. Kunchariyakun, K., Sukmak, P.: Utilization of garnet residue in radiation shielding cement mortar. Constr. Build. Mater. **262**, 120122 (2020)
12. Sirin, M.: The effect of titanium (Ti) additive on radiation shielding efficiency of $Al_{25}Zn$ alloy. Prog. Nucl. Energy. **128**, 103470 (2020)
13. Sayyed, M.I., Mahmoud, K.A., Tashlykov, O.L., Khandaker, M.U., Faruque, M.R.I.: Enhancement of the shielding capability of soda–lime glasses with Sb_2O_3 dopant: a potential material for radiation safety in nuclear installations. Appl. Sci. **2021**(11), 326 (2021). https://doi.org/10.3390/app11010326
14. Kaewjaeng, S., Kothan, S., Chanthima, N., Kimd, H.J., Kaewkhao, J.: Gamma radiation shielding materials of lanthanum calcium silicoborate glasses. Mater. Today: Proc. **5**, 14901–14906 (2018)
15. Hongtong, W., Kaewjaeng, S., Kothan, S., Meejitpaisan, P., Cheewasukhanont, W., Limkitjaroenporn, P., Kaewkhao, J.: Development of gadolinium doped calcium phosphate oxyfluoride glasses for X-ray shielding materials. Mater. Today: Proc. **5**, 14063–14068 (2018)
16. Sayyed, M.I., Almuqrin, A.H., Kurtulus, R., Javier-Hila, A.M.V., Kaky, K., Kavas, T.: X-ray shielding characteristics of P_2O_5–Nb_2O_5 glass doped with Bi2O3 by using EPICS2017 and Phy-X/PSD. Appl. Phys. A. **127**, 243 (2021)
17. KA Naseer, K. Marimuthu: The impact of Er/Yb co-doping on the spectroscopic performance of bismuth boron phosphate glasses for photonic applications. Vacuum, In press. https://doi.org/10.1016/j.vacuum.2020.109788.
18. Komatsu, T., Dimitrov, V., Tasheva, T., Honma, T.: A review: a new insight for electronic polarizability and chemical bond strength in Bi_2O_3-based glasses. J. Non-Cryst. Solids. **550**, 120365 (2020)
19. Hendi, A.A., Rashad, M., Sayyed, M.I.: Gamma radiation shielding study of tellurite glasses containing V_2O_5 and Bi_2O_3 using Geant4 code. Ceram. Int. **46**, 28870–28876 (2020)

20. Almuqrin, A.H., Sayyed, M.I., Kumar, A., El-bashir, B.O., Akkurt, I.: Optical, mechanical properties and gamma ray shielding behavior of TeO_2-Bi_2O_3-PbO-MgO-B_2O_3 glasses using FLUKA simulation code. Opt. Mater. **113**, 110900 (2021)
21. Kaur, R., Bhatia, V., Kumar, D., Rao, S.M.D., Singh, S.P., Kumar, A.: Physical, structural, optical and thermoluminescence behavior of Dy_2O_3 doped sodium magnesium borosilicate glasses. Results Phys. **12**, 827–839 (2019)
22. Kumar, A., Kaur, R., Sayyed, M.I., Rashad, M., Singh, M., Ali, A.M.: Physical, structural, optical and gamma ray shielding behavior of (20+ x) PbO–10 BaO–10 Na_2O–10 MgO–(50-x) B_2O_3 glasses. Phys. B Condens. Matter. **552**, 110–118 (2019)
23. Laariedh, F., Sayyed, M.I., Kumar, A., Tekin, H.O., Kaur, R., Badeche, T.B.: Studies on the structural, optical and radiation shielding properties of (50–x) PbO–10 WO_3–10 Na_2O–10 MgO–(20+ x) B_2O_3 glasses. J. Non-Cryst. Solids. **513**, 159–166 (2019)
24. Ali, A.M., Sayyed, M.I., Kumar, A., Rashad, M., Alshehri, A.M., Kaur, R.: Optically transparent newly developed glass materials for gamma ray shielding applications. J. Non-Cryst. Solids. **521**, 119490 (2019)
25. Sayyed, M.I., Laariedh, F., Kumr, A., Al-Buriahi, M.S.: Experimental studies on the gamma photons-shielding competence of TeO_2–PbO–BaO–Na_2O–B_2O_3 glasses. Appl. Phys. A. **126**, 4 (2019)
26. X-5 Monte Carlo Team, MCNP-a General Monte Carlo N-Particle Transport Code, Version 5, Los Alamos Controlled Publication. LA-CP-03-0245. 2003.
27. M.J. Berger, J H. Hubbel, S.M. Seltzer, J. Chang, J.S. Coursey, R. Sukumar, DS. Zucker, XCOM: Photon Cross Sections Database, 2010. https://doi.org/10.18434/T48G6X
28. Naseer, K.A., Marimuthu, K., Al-Buriahi, M.S.: Amani Alalawi, HO Tekin, Influence of Bi_2O_3 concentration on barium-telluroborate glasses; physical, structural and radiation shielding properties. Ceram. Int. **47**, 329–340 (2021)
29. Naseer, K.A., Arun Kumar, S., Marimuthu, K.: The impact of Er^{3+} ions on the spectroscopic scrutiny of bismuth bariumtelluroborate glasses for display devices and 1.53 μm amplification. J. Non-Cryst. Solids. **520**, 119463 (2019)
30. Hivrekar, M.M., Sable, D.B., Solunke, M.B., Jadhav, K.M.: Network structure analysis of modifier CdO doped sodium borate glass using FTIR and Raman spectroscopy. J. Non-Cryst. Solids. **474**, 58–65 (2017)
31. Coelho, J., Freire, C., Hussain, N.S.: Structural studies of lead lithium borate glasses doped with silver oxide. Spectrochim. Acta A Mol. Biomol. Spectrosc. **86**, 392–398 (2012)
32. Djamal, M., Yuliantini, L., Hidayat, R., Rauf, N., Horprathum, M., Rajaramakrishna, R., Boonin, K., Yasaka, P., Kaewkhao, J., Venkatramu, V., Kothan, S.: Spectroscopic study of Nd^{3+} ion-doped Zn-Al-Ba borate glasses for NIR emitting device applications. Opt. Mater. **107**, 110018 (2020)
33. Khan, S., Kaur, G., Singh, K.: Effect of ZrO_2 on dielectric, optical and structural properties of yttrium calcium borosilicate glasses. Ceram. Int. **43**, 722–727 (2017)
34. El-Maaref, A.A., Shaaban, K.H.S., Abdelawwad, M., Saddeek, Y.B.: Optical characterizations and Judd-Ofelt analysis of Dy^{3+} doped borosilicate glasses. Opt. Mater. **72**, 169–176 (2017)
35. Schott AG, Schott-radiation shielding glass, version May 2013. www.schott.com/advanced_optics
36. K A Mahmoud, M I Sayyed, Abdullah M Alhuthali, M Y Hanfi: The effect of CuO additive on the mechanical and radiation shielding features of $Li_2B_4O_7$-Pb_2O_3 glass system. Boletín de la Sociedad Española de Cerámica y Vidrio, 2021, In Press https://doi.org/10.1016/j.bsecv.2020.11.005